Electronic Supporting Information

Synthesis and Experimental Details

Materials

Palladium (II) nitrate solution (12-16% Pd) and a range of metal salts (ammonium tetrachloroplatinate (II), sodium tetrachloroaurate (III), ruthenium (III) chloride trihydrate and tellurium tetrachloride) were purchased from Alfa Aesar. Johnson Matthey provided Norit GSX activated charcoal and Iridium (III) chloride. Polyvinylpyrrolidone (PVP, M_w=40,000), formic acid (98%), and a range of metal salts (Cobalt (II) nitrate hexahydrate, silver (I) nitrate, tin (II) chloride dihydrate, bismuth (II) nitrate pentahydrate and antimony (III) chloride) were purchased from Sigma-Aldrich. Copper (II) nitrate and Lead (II) nitrate were purchased from BDH. All other solvents and reagents were purchased from Sigma-Aldrich and used as received.

Synthesis of Pd-PVP

Polyvinylpyrrolidone (PVP) stabilized palladium nanoparticles (Pd-PVP) were synthesized using a modified polyol method used by Bonet et al.[S1] Typically, 0.040 g (0.15 mmol) of $Pd(NO_3)$ and 0.166 g of PVP were dissolved in 30 mL of ethylene glycol, by sonication for 5 min, resulting in a 1:10 ratio of moles of metal to PVP monomer units. The light brown solution was heated to the 120°C at 5°C/min under a nitrogen atmosphere and kept there for 1.5 hours, turning dark brown as the colloidal nanoparticles (test solution) are formed. Once cooled to room temperature, the particles were mixed with acetone and centrifuged to precipitate the nanoparticles. The sample was then washed three times with acetone and dried at room temperature in air

Decoration of Pd-PVP

The colloidal nanoparticles, Pd-PVP, were decorated using the polyol reduction method.[S1] A sample of Pd-PVP nanoparticles synthesized as above, but not precipitated. After the sol cooled to room temperature, hydrogen was flown through for 30 minutes. The required molar ratio of decorating metal salt was dissolved in 5 mL of ethylene glycol and added to the flask, which was stirred for 15 min before being heated up to 120°C as above before being precipitated, washed and dried.

For hydrazine reduction or $NaBH_4$ reduction for the insoluble Te samples and some Ag samples, after adding the required quantity of metal salt precursor (insoluble $TeCl_4$ salt to soluble Te^{2+}) and stirring for 15 min, a 4 times excess of reducing agent was dissolved in 5 mL of ethylene glycol and added drop-wise to the reaction mixture. After adding the reducing agent the mixture was left to stir for 1 hour before being precipitated, washed and dried as above.

Synthesis of Pd/C

Carbon supported palladium nanoparticles (Pd/C) were synthesized using a hydrogen gas reduction method. 0.3 g of GSX Norit carbon and $Pd(NO_3)_2$ solution (mass required to produce 10% wt. Pd) were mixed in 200 mL of water. The pH of the solution was adjusted to 11 by drop-wise addition of NaOH solution. The mixture was stirred vigorously and bubbled with nitrogen for 30 minutes before switching to hydrogen for 1 hour at room temperature. The sample was then filtered using a 0.2 μm membrane filter and washed with de-ionised water until neutral. Then the sample was dried overnight at 100°C.

Decoration of Pd/C

For decoration of Pd/C, 0.2 g of 10% Pd/C was dispersed in 120 mL of water, by sonication, and the pH of the sample varied if necessary. The sample was then treated under hydrogen for 30 minutes before the required molar ratio of metal salt (for the desired coverage of Pd) was dissolved in 5 mL of H_2O, or a solution of nitric acid or sodium hydroxide if necessary and added to the dispersed Pd/C. The salt was added to the flask and the contents stirred for 15 minutes allowing deposition using a redox interaction between the metal salt and the pre-reduced Pd surface reported by Gauthard et al..[S2] A 4:1 excess of reductant was dissolved in a further 5 mL of H_2O and added to the mixture and left to stir for 1 hour at room temperature. The resulting sample was filtered and dried as for the Pd/C.

Catalyst Characterization

XRD analysis was performed using a PANalytical X'Pert Pro diffractometer, operating in Bragg-Brentano focusing geometry and using $Cu_{K\alpha}$ radiation (λ = 1.5418 Å) from a generator operating at 40 kV and 40 mA. Colloidal samples were prepared by dispersing the samples in water and this was dropped onto a glass slide to form a thin film. For supported catalysts the powder was placed directly onto a glass slide and smoothed to form a thin uniform layer. Size was calculated from the Pd (220), as this does not overlap with any other peak, using the Scherrer equation. Infrared data was collected using a Nicolet 6700 ATR-IR spectrometer with a liquid-nitrogen-cooled MCT detector. A 150μL of test sample was placed on a smart golden gate-ZeSe/diamond crystal surface and evaporated under nitrogen. The spectra were obtained by averaging 128 scans with a resolution of 4 cm^{-1} over wavenumbers ranging from 650 to 4000 cm^{-1}. For CO adsorption, samples containing $0.15x10^{-3}$ moles of Pd were dissolved in approx. 2 mL water and 1%CO in N_2 was then bubbled through for 30 mins. Surface area was measured by CO chemisorption, the sample was first pre-treated with hydrogen, to simulate the conditions of the reaction, then pure CO was pulsed over the sample and the amount of CO adsorbed was measured by a temperature conductivity detector. Surface Area was calculated by assuming a chemisorption stoichiometry of CO/Pd=1 and a Pd surface packing of $1.27x10^{19}$ as used by Mahata and Vishwanathan.[S3] TEM was performed on a JOEL 2010 running at 200 kV, EDX is performed using an Oxford Instruments LZ5 windowless energy dispersive X-ray spectrometer. Samples for TEM were prepared by dispersing the dry catalyst in ethanol using sonication then a drop was paced on a holey-carbon coated copper grid. The grid was then dried at under vacuum for at least 1 hour.

HRTEM/STEM and Crystal Simulation and Analysis

Further detailed microscopic analysis was carried out by accessing Birmingham University JEOL-JEM2100 Aberration-Corrected Transmission Electron Microscope using the following instrumental conditions: Voltage (kV) 200; a bright-field imaging in scanning mode using an on-axis detector which is capable of atomic resolution imaging; a dark-field (Z-contrast) imaging in scanning mode using an off-axis annular detector which is capable of atomic-resolution imaging; compositional analysis by X-ray emission detection in the scanning mode. Particular care was exercised to minimize any beam damage or adatoms reconstruction by using low tip emission current and short exposure time where background signals and time changes were recorded and compared. The simulation of cubo-octohedral PdBi (edge/corner site blockage) and PdTe (face site blockage) models for STEM images was approached in the following manner: First, the atomistic model was constructed using a home built code to take in consideration corner, edge, face and terrace sites using Pd FCC as the lattice constant - 3.89Å; Bi assumes FCC epitaxial growth on edge and corn sites with the same lattice constant; Te assumes FCC epitaxial growth on faces with the same lattice constant. This is the simplest approximation using atomic form factor: EJK.

XRD

The PdBi alloy peaks were calculated using Vegards Law by assuming an FCC structure, utilising the known stoichiometric ratio of Pd and Bi and the bond length of bulk Pd and Bi. The strained Ag@Pd core-shell structure was simulated by constructing a strained core-shell nanoparticle using a modified method of Fairclough et al. and simulating the resulting XRD patterning using a program of 'DISCUS' using a Cu k alpha source.[S4,S5]

The parameters used:

Table S1 - Crystal structures & basic physical properties of metals

	Pd	Ag
Crystal Structure	FCC	FCC
Lattice constant (Å)	3.8907	4.090
Bulk Modulus (GPa)	180	100
Young's Modulus (GPa)	121	83
Poisson Ratio	0.39	0.37

Activity Testing

For supported catalysts, approximately 42.5 mg of Pd/C was added to a reaction vessel under a nitrogen atmosphere to which 10.575 mL of 1.4M formic acid was added. For colloidal catalysts, samples containing $0.15x10^{-3}$ moles of Pd were dispersed in 5 mL of water and added to a reaction vessel under nitrogen to this formic acid was solution was added to produce 15.860 mL of 1.4M formic acid. Reaction vessels were then stirred at 1000 rpm and gas production was measured by water displacement in an upturned burette. For analysis of the gas, a reactor was prepared as above and the gas collected by syringe before being injected into a GC with both a thermal conductivity (TCD) and flame ionization detector (FID) or into a GC-methanator FID. This allows accurate detection of H_2, CO_2, CO and other gases. The detection limit is below 10 ppm for CO, as required to confirm the gas is applicable for hydrogen fuel cell use

Supporting Results

Table S2 - Activity of decorated Pd-PVP nanoparticles 0.15 mmoles Pd in 15.860 mL of 1.4M formic acid

Sample Name	Initial Rate[a] *(L g(Pd)$^{-1}$ min^{-1})*	Final Rate[b] *(L g(Pd)$^{-1}$ min^{-1})*	Deactivation[c] *(I/F Rate)*	Total Gas[d] *(L g(Pd)$^{-1}$)*
Pd-PVP	0.1060	0.0066	16.06	2.81
15%Cu	0.0350	0.0069	5.07	1.67
15%Au	0.0940	0.0066	14.24	2.36
15%Co	0.0350	0.0053	6.60	1.47
15%Sn	0.0490	0.0056	8.75	1.83

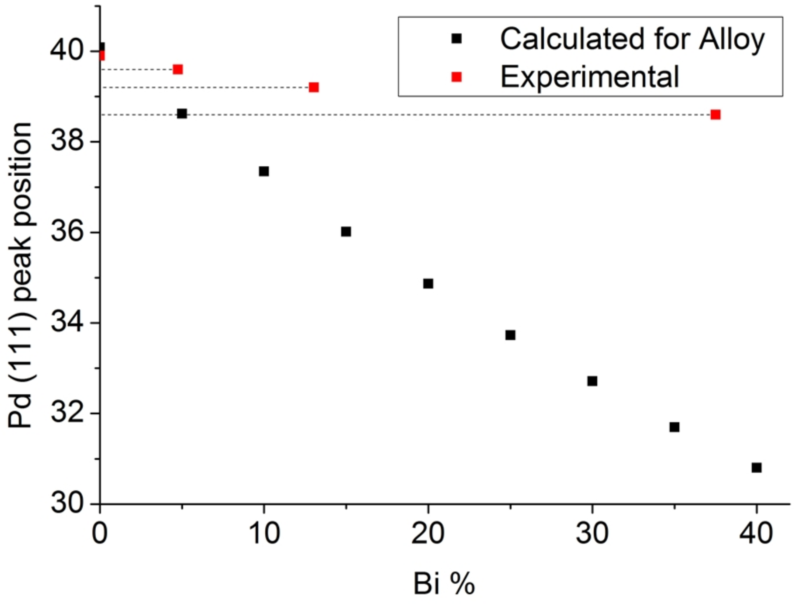

Figure S1 – Pd(111) peak position from XRD against %Bi in sample for various ratios of Pd-PVP+Bi and a calculated alloy.

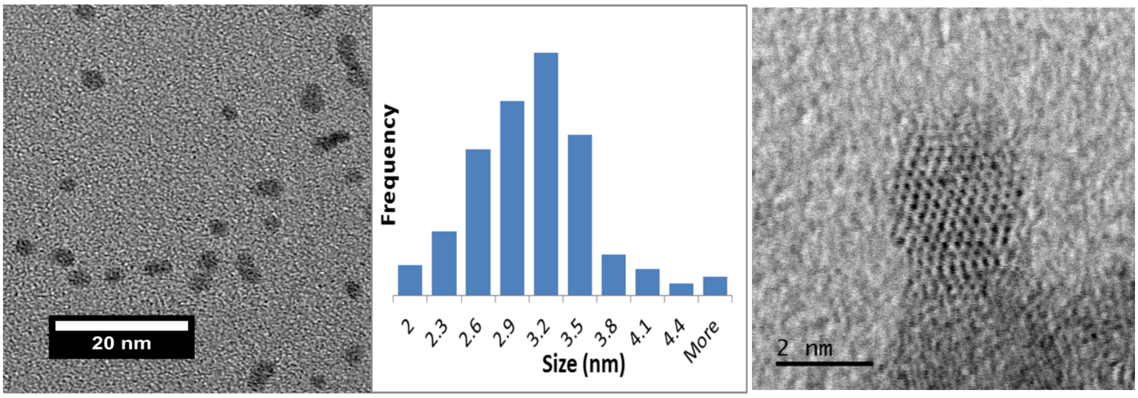

Figure S2 – Low resolution TEM; Size distribution of Pd-PVP with a 1:10 Pd: PVP monomer unit ratio and HRTEM of a selected particle are shown.

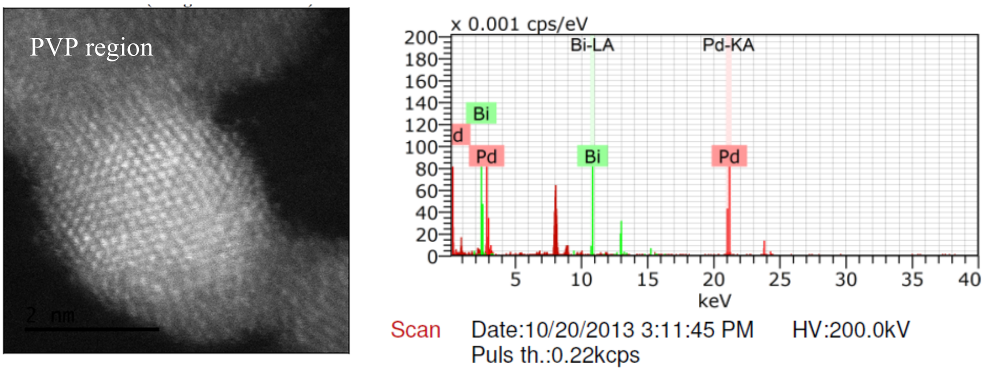

Figure S3 – HADDF image and EDX spectra of Pd-PVP+Bi 1: 0.15 showing a cubooctahedral Pd(Bi) crystal embedded in non-crystalline PVP. It is noted that corresponding bright field image was less capable of differentiating nanocrystals from the PVP.

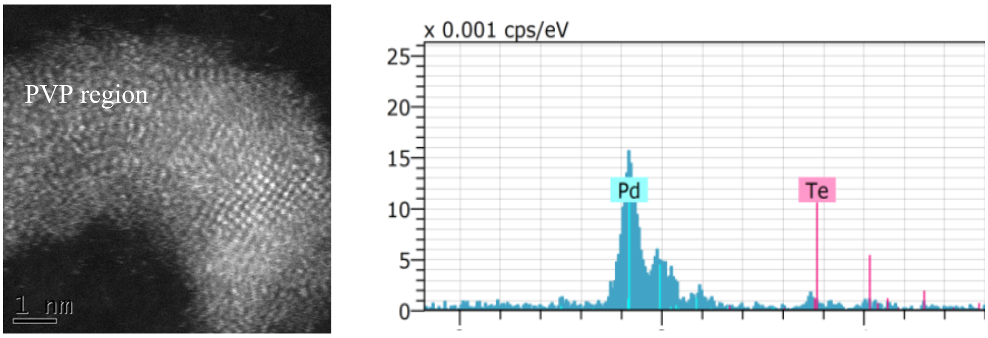

Figure S4 – HADDAF image and EDX spectra of Pd-PVP+Te 1: 0.15 showing a cubooctahedral Pd(Te) crystal embedded in non-crystalline PVP

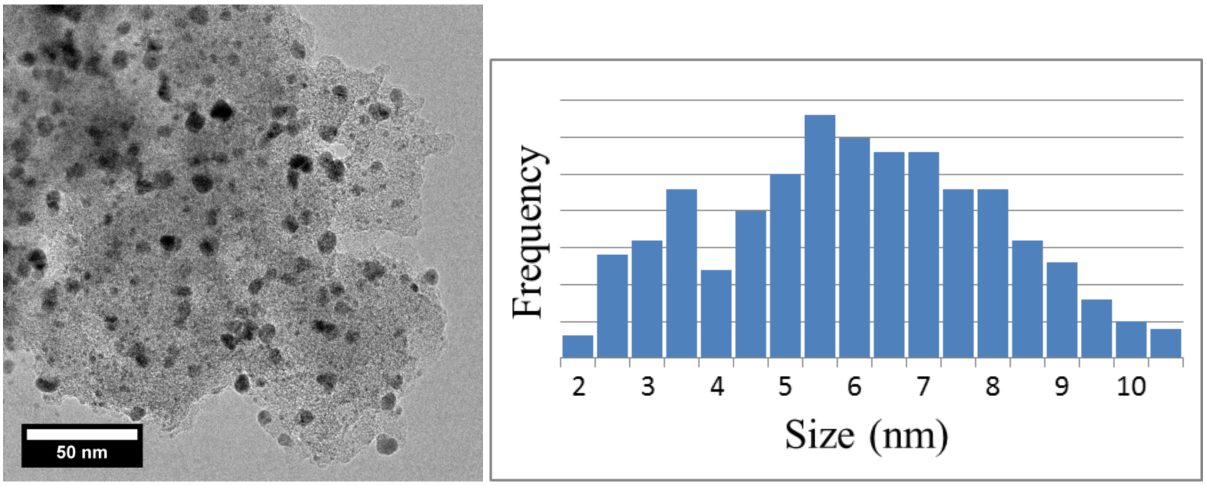

Figure S5 – TEM and size distribution of 10% Pd/C

Table S3 EDX, XRD and TEM of Pd-PVP, Pd-PVP+Bi and Pd/C

Sample	Pd:Bi ratio[a]	Size XRD (nm) [b] +/-0.2 nm	Size TEM (nm)[c]
Pd-PVP	N/A	3.2	2.95
Pd-PVP+Bi 1:0.05	1:0.055	3.3	3.47
Pd-PVP+Bi 1:0.15	1:0.170	3.6	4.93
Pd-PVP+Bi 1:0.6	1:0.47	3.3	6.19
Pd/C	N/A	5.5	5.77

(a) ratio of Pd and Bi from EDX, (b) determined from fitting (220) peak , (c) Particle size from average of at least 200 particles. It is noted that the polymer shell embedding the Pd particles can severely mask the XPS signals of the Pd-PVP samples hence they are not used to derive the Pd/Bi ratios. Instead, EDX is used for the analysis as shown in the second column.

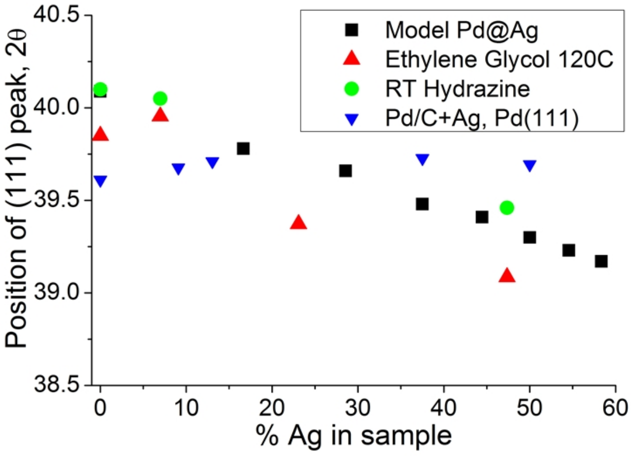

Figure S6 – (111) peak position from XRD against % Ag in sample. For Pd-PVP+Ag (various ratios) with Ag reduction by ethylene glycol at 120°C (Red triangle) or room temperature by hydrazine (Green circles), and

Pd/C+Ag (Blue inverted triangles).

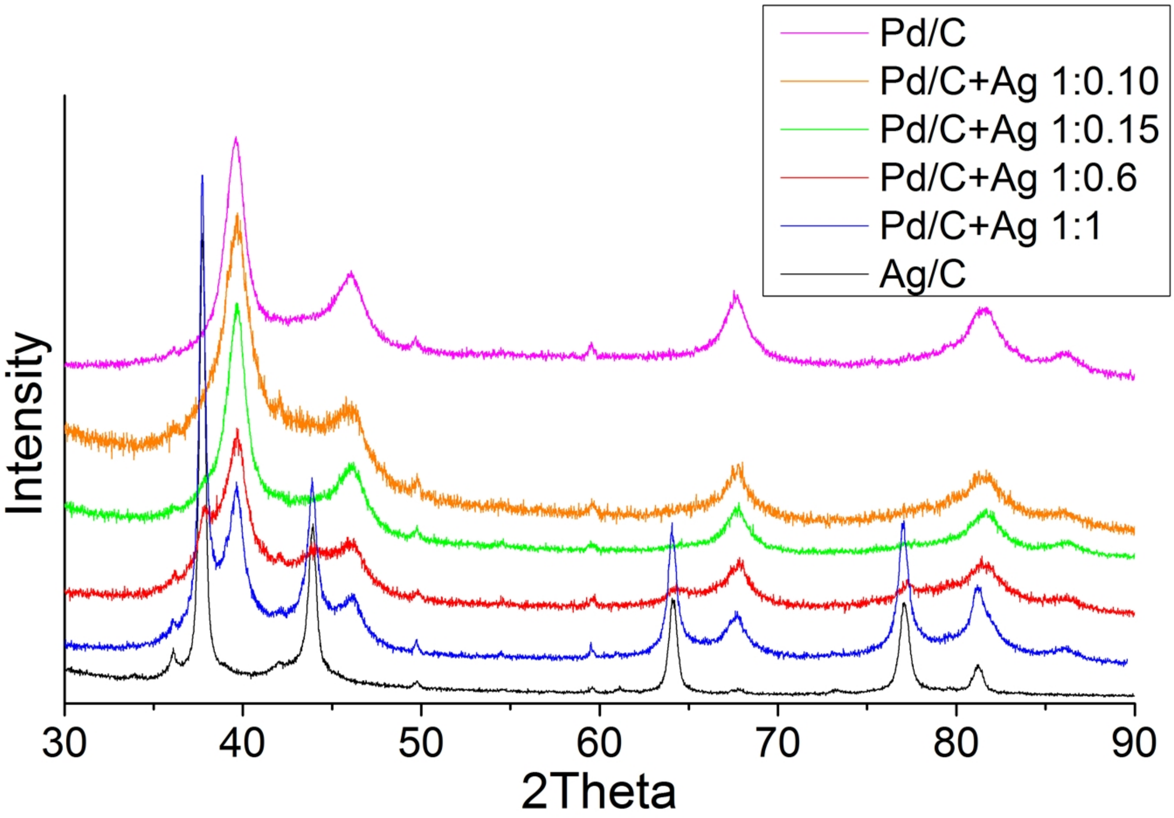

Figure S7 – XRD Pd/C, Ag/C and Pd/C+Ag various ratios

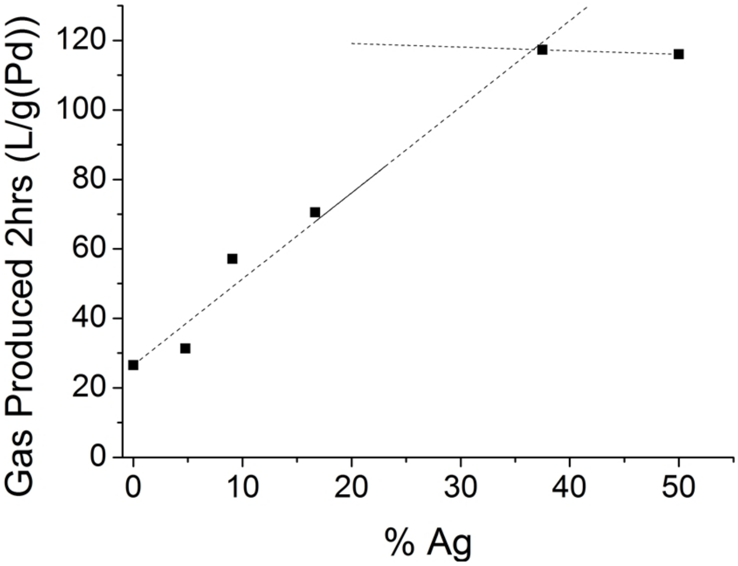

Figure S8 – Formic acid decomposition activity of Pd/C+Ag various ratios over 2 hours

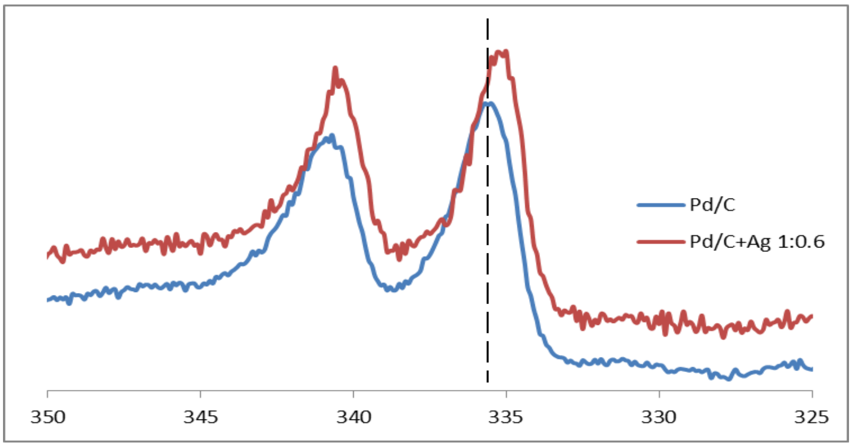

Figure S9 – XPS of Pd 3d region of Pd/C and Pd/C+Ag 1:0.6 ratio of Pd to Ag showing a clear shift in binding energies of Pd by Ag doping

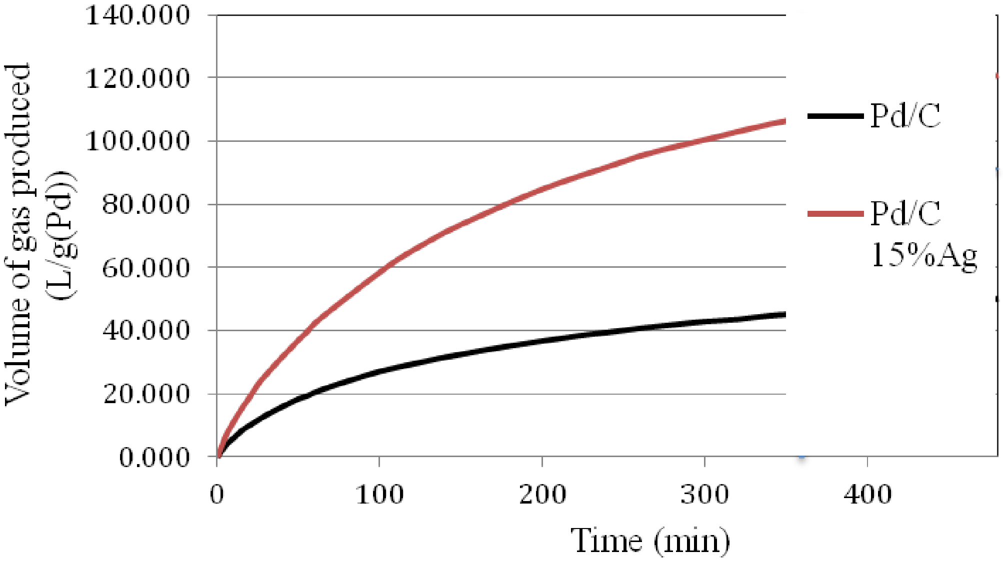

Figure S10– Activity of Pd/C and Pd/C+Ag 1:0.15 tested over an extended period. 4.25 mg Pd stirred in 10.575 mL of 1.4M formic acid at 25°C

Table S4 – Analysis of long testing Pd/C and Pd/C+Ag 1:0.15. 4.25 mg Pd stirred in 10.57 5mL of 1.4M formic acid at 25°C

Sample		Pd/C	Pd/C+Ag 1:0.15
Initial Rate	*(L g(Pd)$^{-1}$ min^{-1})*	0.612	1.134
Rate at 2hrs	*(L g(Pd)$^{-1}$ min^{-1})*	0.113	0.313
2hr Deactivation	*(Int./Fin. Rate)*	5.417	3.624
Rate at 4hrs	*(L g(Pd)$^{-1}$ min^{-1})*	0.061	0.168
2-4hr Deactivation	*(Int./Fin. Rate)*	1.846	1.860
Rate at 6hrs	*(L g(Pd)$^{-1}$ min^{-1})*	0.033	0.096
4-6hr Deactivation	*(Int./Fin. Rate)*	1.857	1.744
0-6hr Deactivation	*(Int./Fin. Rate)*	18.571	11.756

STEM Simulation and analysis:

PdTe

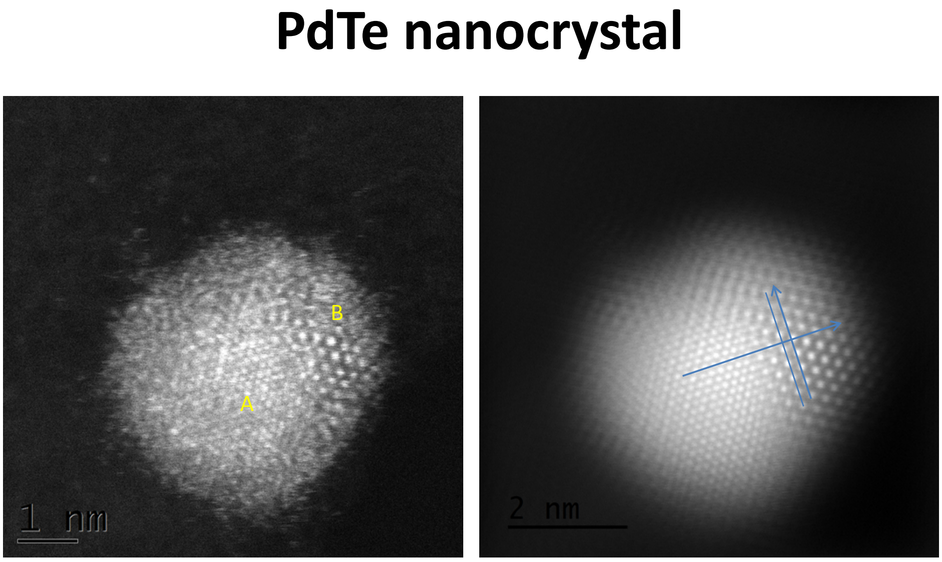

Original HAADF image **FFT filter HAADF image**

Figure S11– Original HAADF image and Fourier transformed filtered image of PVP+Te 1: 0.15 showing a single cubooctahedral Pd(Te) crystal

As seen from the High-Angle Annular Dark Field (HADDF) image that there are two distinctive types of lattices observed in a single particle. The inner crystal with smaller lattice (labeled as A) is covered with a larger lattice (labeled as B) (EDX confirms both Pd and Te signals). The inner crystal lattice is coherent with the outer surface lattice which has a larger parameter. It should be noted that the d-spacing of the outer surface lattice fits with the Te hcp structure whereas the inner crystal fits with Pd fcc structure.

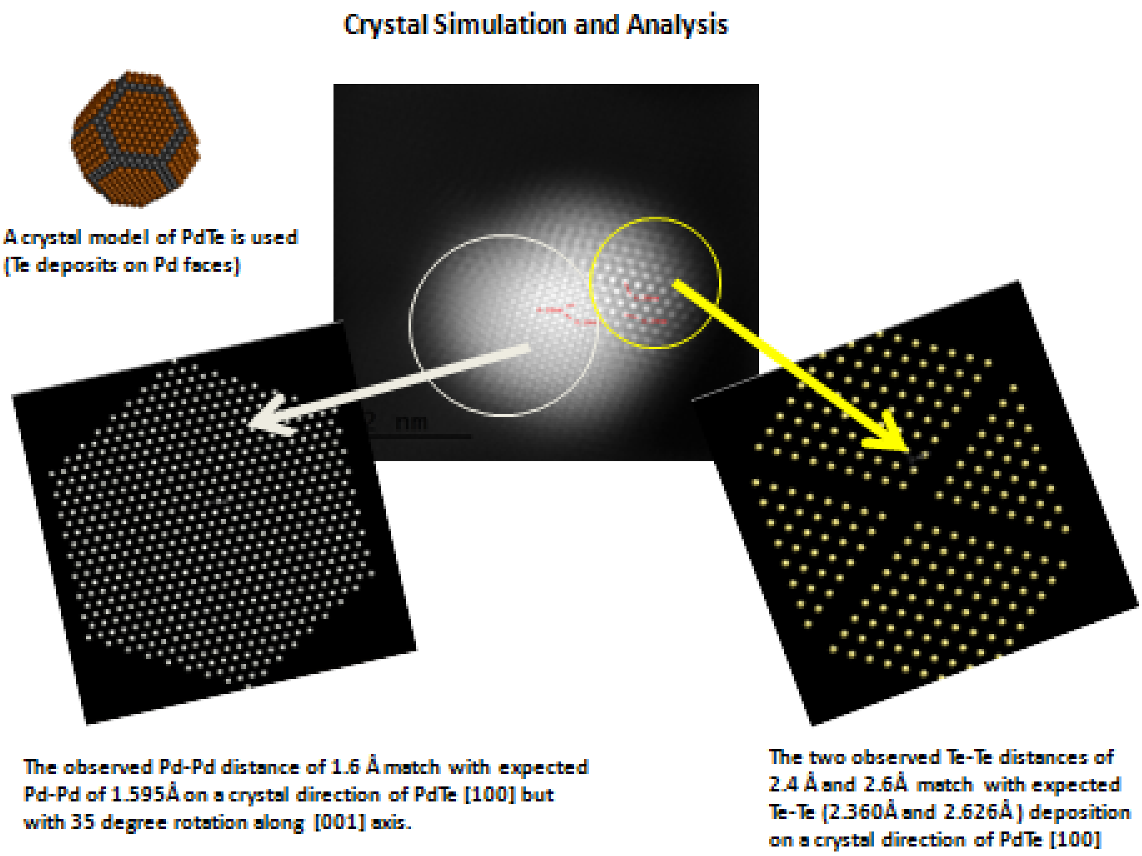

Crystal Simulation and Analysis

A crystal model of PdTe is used (Te deposits on Pd faces)

The observed Pd-Pd distance of 1.6 Å match with expected Pd-Pd of 1.595Å on a crystal direction of PdTe [100] but with 35 degree rotation along [001] axis.

The two observed Te-Te distances of 2.4 Å and 2.6Å match with expected Te-Te (2.360Å and 2.626Å) deposition on a crystal direction of PdTe [100]

Figure S12– Analysis of patterns and atomic spacings of a single cubooctahedral Pd(Te) crystal with our face doped PdTe model

Using crystal simulation and analysis of the d-spacings of Pd-Pd and Te-Te observed in the HADDF image the results match well with the expected Pd-Pd distance and Te-Te distances with our face deposition model of PdTe indicative of an extensive growth of the Te surface lattice (at least 7 atoms width) on the face of Pd cubooctahedral crystal. It is therefore this model supports our postulation of face deposition of Te atoms on Pd crystal. However, the Pd and Te lattices cannot be matched with the same crystals orientation at the interface. It is evident that the outer shell of Te layers has 35 degree mismatch with the core Pd as compared to the PdTe crystal simulation. But, there is no mismatch within Pd lattice and Te lattice in the HAADF image since both the Pd and Te atom arrays are fitted relatively well in the lines (as shown in both blue lines above). It is not yet known how the atoms at the interface of the two low index planes are arranged.

PdBi

PdBi nanocrystal

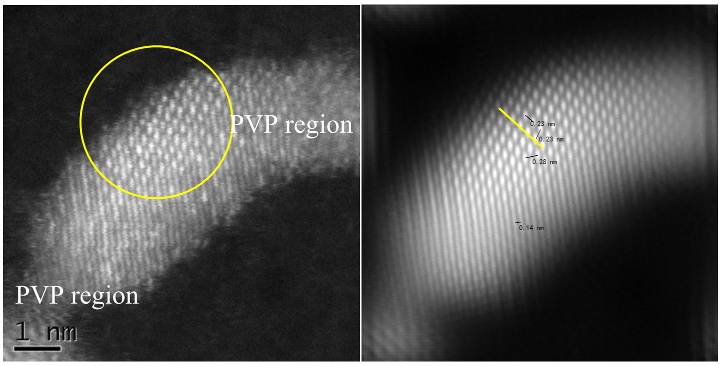

Original HAADF image **FFT filter HAADF image**

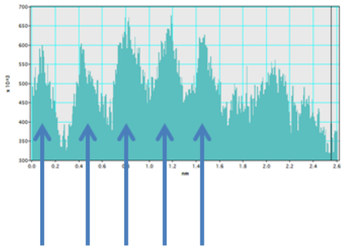

A line profile along the yellow line marked showing five distinct larger atoms on a crystal surface, each with a half peak width of 1.6Å (match with Bi atomic radius) on Pd crystal with smaller atom size (Pd atomic radius 1.4 Å). Scale bar, 1 nm. The intensities of the first 5 peaks are in the range between 600-650 relative values above the background of 550.

Figure S13– Original HAADF image and FFT filtered image of PVP+Bi 1: 0.15 showing a single cubooctahedral Pd(Bi) crystal partially covered with PVP; line scan profile along the marked yellow line of Bi atoms

In contrast to the PdTe we did not find extensive deposition with surface lattice of Bi atoms but instead individual Bi atoms selectively deposition on a upper part (yellow circle) of Pd lattice were found. Particularly care was paid to reduce the surface reconstruction (migration) of these adatoms by the low beam irradiation at short exposure time. A typical low energy high-angle annular dark field image of a Pd crystal doped with Bi (EDX confirms both Pd and Bi signals) with fourier transformation and a corresponding line profiling on the surface deposition are shown in Fig. S13. Since atomic number of Bi is higher than Pd and Bi would appear brighter than Pd. This was indeed observed in HAADF image and line scan as above. It is interesting to see the specific dwelling of these adatoms on the Pd nanocrystal. From the crystal simulation and analysis (figures below) it can be concluded that Bi atoms form deposition on the Pd with the Bi atoms are indeed found around the edge/corner regions of the [110] orientation of the model PdBi.

Crystal Simulation and Analysis

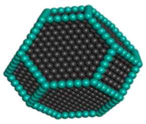

A crystal model of PdBi is used (Bi deposits on Pd edges and corners)

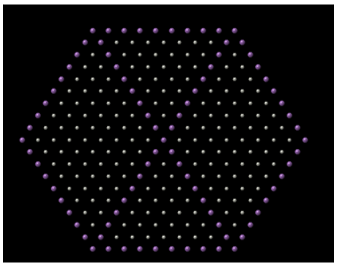

The Bi atoms appear to fit the edge regions in [110] PdBi model.

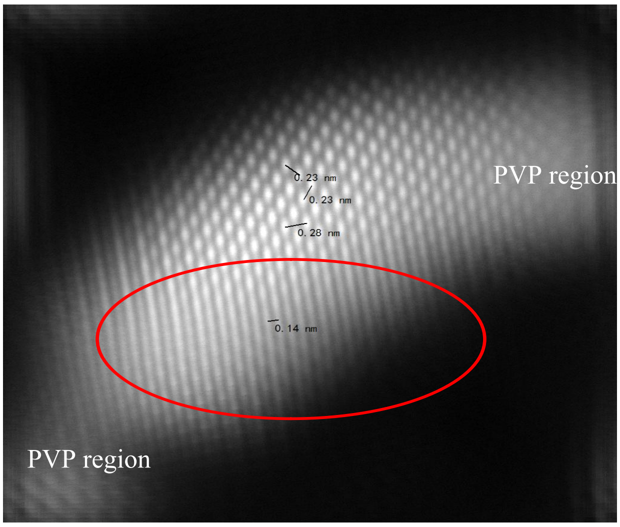

However, the bottom of the crystal shows fringes with fring separation of 0.14nm instead of individual atoms.

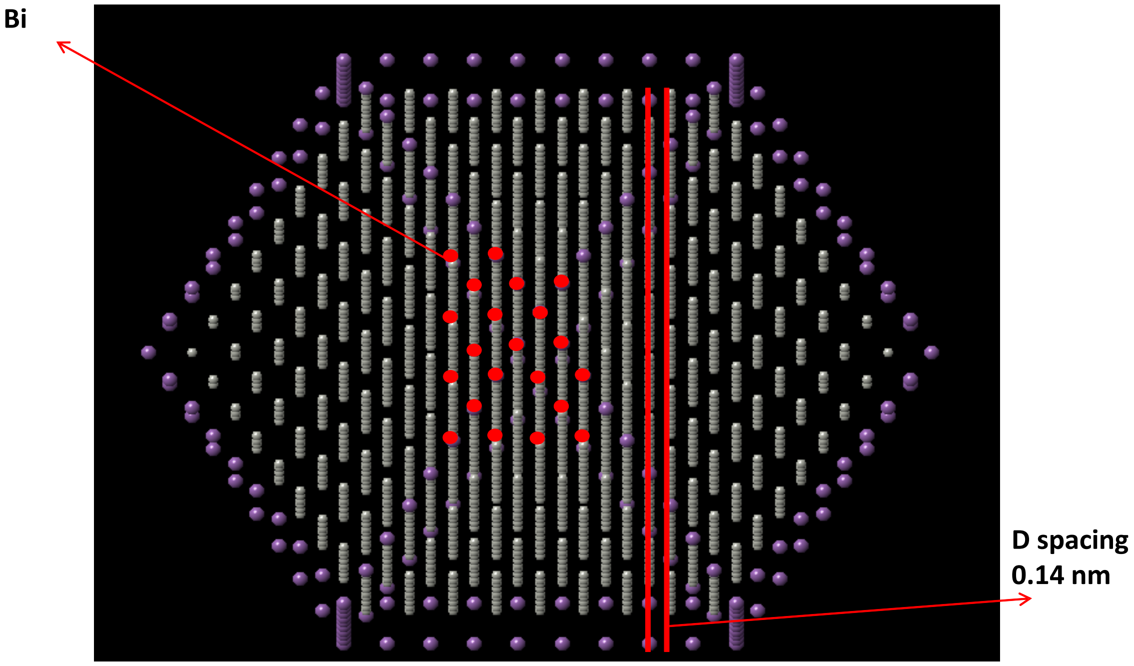

By tilting few degrees from [110] on our PdBi model, it is found that the d spacing of 0.14 nm matches with the fringe separation observed from bottom of the crystal by HAADF image. The brighter Bi atoms on top of the crystal with observed atom distances of 0.23nm, 0.23nm, 0.28nm (labelled) are found on the edge regions with respect to our PdBi model.

Figure S14– Analysis of patterns and atomic distances of a single cubooctahedral Pd(Bi) crystal with our edge/corner doped PdBi model

We have marked down all the individual Bi atoms observed with reference to the Pd crystal as seen in Fig. S14. Notice that 18 of the 21 observed Bi atoms (red) are located on the double-edge atom positions (purple) along the tilted [110] direction. This supports our Bi decorated model on corner/edge derived from the corresponding activity study. There are 3 Bi atoms located in other non-edge positions, rendering the deposited Bi atoms appeared as 2-D arrays in this region. We believe that these arrays with more favourable packing are the result of the extended growth of Bi atoms from the edge positions or defect regions. Further study on the growth of deposited Bi will be carried out. Thus, from these above detailed HRTEM and STEM and crystal simulations the results are consistent with our proposed models of selective depositions derived from the catalytic works as well as CO chemisorption experiments.

PdAg

Our CO adsorption work suggests that the PdAg nanoparticle surface is quite complex, which in general agrees with the recent and extensive studies on both PdAg nanoparticle (defective core shell due to a mismatch of lattices) or Ag atoms deposition on extended Pd reported in the literature [S6,S7]. Accordingly, the surface from the deposition of Ag atoms on Pd is characterised with Pd and Ag surface atoms almost randomly distributed in the topmost bimetallic layer as also suggested by our present work. There are also ensembles of Ag (as islands), Pd and alloy on the surface. According to Behm, and co-workers [S6] i) CO binding strength on Pd decreases significantly with increasing Ag concentration (electron effect as also evidenced from our work), and that ii) CO will preferentially adsorb on atomic islands with a certain size. It is interesting from our work that the increase in Ag deposition could give levelled promotion effect at about 50%. It is thought that the Ag deposition will reduce the number of surface sites but can also form 3-D islands and alloy ensembles at high coverage.

Due to the extensive characterization of this nanoparticle and the extremely weak contrast difference between Ag and Pd, we did not perform the STEM analysis.

As a result, in this paper, we propose that the atomic location of metal precursors on the Pd crystal is primarily driven by their total adsorption energy. Such that the lone pair electrons of the metal precursors maximize their interaction with the surface Pd atoms in a specific mode. On the other hand, the use of strong $NaBH_4$ as reductant and their storage in hydrogen under the reaction conditions should keep them in metallic state. Thus, the atomic size and packing of Bi and Te derived from STEM match to their zero oxidation state.

$^{12}CO/^{13}CO$ adsorption ATR-FTIR test: Dipole-dipole coupling effect evaluation

Previous work has demonstrated FTIR of CO adsorption to be an effective technique for investigating electronic modification of the metal surface by examining the degree of CO adsorption band shift [S8]. However, the dipole-dipole CO-CO interactions at different CO partial pressure and different surface metal site concentration can have their effect on band frequency. We have therefore used a fixed and low partial pressure of CO for all the measurements. In order to assess that the extent of a maximum band shift effect due to dipole-dipole interaction at decreasing metal site concentration owing to the doping, we have estimated the ^{12}CO-^{12}CO dipole interaction at different site concentrations by the use of ^{13}CO dilution at the site saturation point as shown in Figures S15 and S16 (^{12}CO-^{13}CO is small and can be ignored)[S7]. The adsorption samples were prepared by mixing fixed amount of as-prepared Pd-PVP colloid with aqueous solution of $H^{12}COOH$ and $H^{13}COOH$. The ratio between $H^{12}COOH$ and $H^{13}COOH$ was established according to the volume. The mixture was then rapidly heated up to 100°C to cause dehydration and kept until no gas was produced, which means the Pd sites were fully covered with CO. Pd-PVP samples with different $^{12}CO/^{13}CO$ coverage were achieved by tuning the $H^{12}COOH$/ $H^{13}COOH$ ratio (e.g. using 50% $H^{12}COOH$ + 50% $H^{13}COOH$ to get 50% ^{12}CO with 50% ^{13}CO). The black solution was then dried on the ATR crystal under N_2 and measured at room temperature.

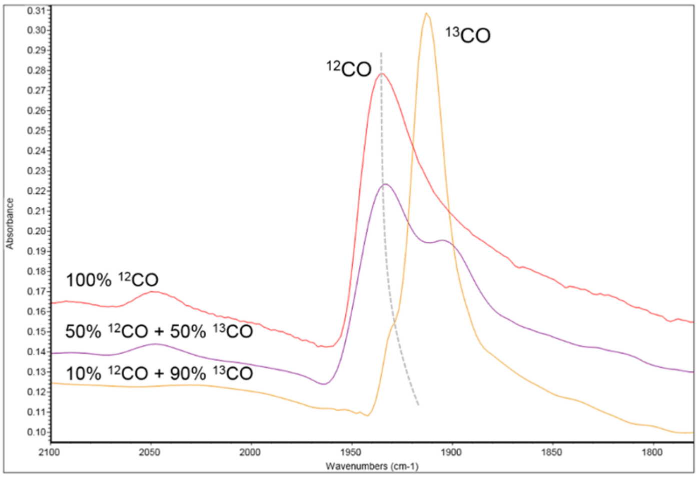

Figure S15 ATR-IR spectra of ^{12}CO+^{13}CO adsorption on Pd-PVP nanoparticles. From top to bottom curves, Pd-PVP nanoparticles were treated with increasing ^{13}CO and decreasing ^{12}CO until the all metal sites saturation with the ^{12}CO or ^{13}CO or their mixtures. With the coverage of ^{12}CO decreased, the bridge adsorption peak of ^{12}CO red shifted, from 1939 cm^{-1} (100% ^{12}CO) to 1925 cm^{-1} (10% ^{12}CO + 90% ^{13}CO). Meanwhile, the bridge adsorption peak of ^{13}CO appeared at 1908 cm^{-1} (50% ^{12}CO+ 50% ^{13}CO) and 1916 cm^{-1} (10% ^{12}CO + 90% ^{13}CO).

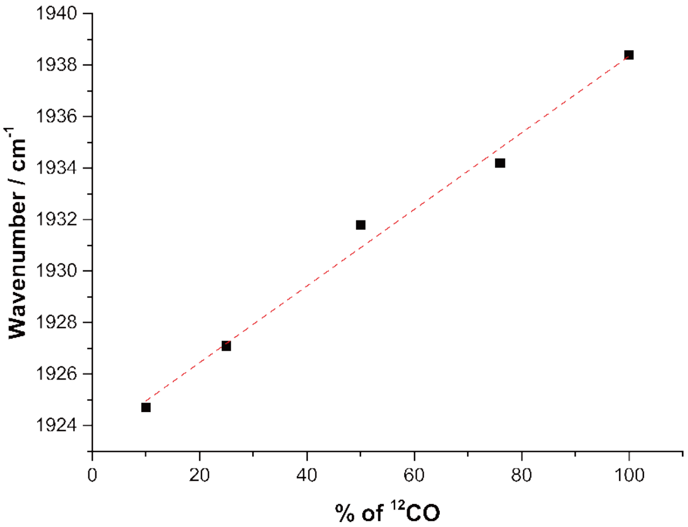

Figure S16 Relationship between ^{12}CO coverage on Pd-PVP nanoparticles and its corresponding ^{12}CO bridge adsorption bands. Thus the correlation equation is:
[^{12}CO bridge adsorption wavenumber]=1923.5+0.1488*[% of ^{12}CO]

As a result, the degree of band shift due to dipole-dipole coupling effect of CO adsorption can be compared to those observed in both Bi and Ag doping to Pd. With 10% Bi doping (1:0.1 molar ratio), 30% of surface metal sites decrease should have caused a maximum red shift of the CO bridge adsorption peak to 1934 cm^{-1} according to the correlation equation in Figure S16 as compared to actual observed shift of 1925 cm^{-1} with a greater extent. With addition of Ag with a ratio of 1:0.15 to Pd, ~40% Pd metal sites are covered, the bridge peak should have shifted to the maximum of 1932 cm^{-1} due to dipole-dipole effect, but the actual peak is located at 1919 cm^{-1}. This clearly suggests that the saturated dipole-dipole effect of CO can only cause smaller shifts but the electronic donation caused by Bi and particularly the Ag doping is the major effect (Ag creates a larger shift than Bi).

References for Supporting Information

[S1] F. Bonet et al. Nanostruct. Mater. **1999**, 11, 1277-1284

[S2] F. Gauthard, F. Epron, J. Barbier J. Catal. **2003**, 220, 182-191

[S3] N. Mahata and V. Vishwanathan J. Catal. **2000**, 196, 262-272

[S4] S. Fairclough et al. J. Phys. Chem. C **2012**, 116, 26898-26907

[S5] T. Proffen and R.B. Neder J. Appl. Cryst. **1997**, 30, 171-175

[S6] J. Gong, F. Zhou, Z. Li and Z. Tang, *Chem. Commun.,* **2013**, 49, 4379-4381

[S7] A. K. Engstfeld, H. E. Hoster, and R. J. Behm, Phys. Chem. Chem. Phys., **2012**, 14, 10754-10761; A. P. Farkas, T. Diemant, J. Bansmann, and R. J. Behm,, ChemPhysChem, **2012**, p. doi: 10.1002/cphc.201200477.

[S8] A. Ortega, F. M. Hoffman, A. M. Bradshaw, *Surf. Sci.* **1982**, *119*, 79–94.